PCCP

Accepted Manuscript

ROYAL SOCIETY OF CHEMISTRY

www.rsc.org/pccp

Physical Chemistry Chemical Physics
CREATED USING THE RSC LaTeX PCCP ARTICLE TEMPLATE – SEE www.rsc.org/electronicfiles FOR DETAILS
ARTICLE TYPE www. rsc.org/xxxxxx | XXXXXXXX

Prediction of two-photon absorption enhancement in red fluorescent protein chromophores made from non-canonical amino acids†

M. Alaraby Salem[a], Isaac Twelves[a] and Alex Brown[a]*

Received Xth XXXXXXXXXX 20XX, Accepted Xth XXXXXXXXX 20XX
First published on the web Xth XXXXXXXXXX 200X
DOI: 10.1039/b000000x

Two-photon spectroscopy of fluorescent proteins is a powerful bio-imaging tool known for deep tissue penetration and little cellular damage. Being less sensitive than the one-photon microscopy alternatives, a protein with a large two-photon absorption (TPA) cross-section is needed. Here, we use time-dependent density functional theory (TD-DFT) at the B3LYP and CAM-B3LYP/6-31+G(d,p) levels of theory to screen twenty-two possible chromophores that can be formed upon replacing the amino-acid Tyr66 that forms the red fluorescent protein (RFP) chromophore with a non-canonical amino acid. The two-level model for TPA was used to assess the properties (i.e., transition dipole moment, permanent dipole moment difference, and the angle between them) leading to the TPA cross-sections determined via response theory. Computing TPA cross-sections with B3LYP and CAM-B3LYP yield similar overall trends. Results using both functionals agree that the RFP-derived model of the Gold Fluorescent Protein chromophore (Model 20) has the largest intrinsic TPA cross-section. TPA was further computed for selected chromophores following conformational changes: variation of both the dihedral angle of the acylimine moiety and the tilt and twist angles between the rings of the chromophore. The TPA cross-section assumed an oscillatory trend with the rotation of the acylimine dihedral, and the TPA is maximized in the planar conformation for almost all models. Model 21 (a hydroxyquinoline derivative) is shown to be comparable to model 20 in terms of TPA cross-section. The conformational study on Model 21 shows that the acylimine angle has a much stronger effect on the TPA than its tilt and twist angles. Having an intrinsic TPA ability that is more than 7 times that of the native RFP chromophore, Models 20 and 21 appear to be very promising for future experimental investigation.

1 Introduction

Fluorescent proteins (FPs) make up a family of homologues of the *Aequorea victoria* green fluorescent protein (avGFP) initially discovered in the 1960s.[1] The FP chromophore is made by a post-translational modification of three precursory amino acids within the protein shell.[2,3] In some FPs, that are of interest in the present study, there is an additional maturation step, resulting in a chromophore with an extra acylimine moiety (see Figure 1 for a depiction of the red FP (RFP) chromophore).[4] The chromophore structure together with the surrounding protein environment influence the photophysical properties of the protein.[5] Modifications to the precursory amino acids have enabled protein engineers to develop a full spectrum of FPs, ranging from blue-to-red fluorescence.[6,7] Currently many photophysical studies on FPs have focused on their one-photon absorption (OPA), with a recent increasing interest in two-photon absorption (TPA) properties.[8,9]

In TPA microscopy, light of longer wavelength (smaller energy) is absorbed, decreasing the chance of irreparable cell damage associated with higher-energy photons and enabling deeper penetration into thick samples. As TPA varies with the square of the incident light intensity, there is less out-of-focus bleaching and more focused imaging.[10,11] This advantage comes at the expense of sensitivity and thus fluorophores with large TPA probabilities (cross-sections) are needed.

There is a known challenge in measuring absolute TPA cross-sections, especially in biological molecules.[9,12] As discussed by Drobizhev et al.,[13] there exists large deviations - up to two orders of magnitude - between TPA cross-section mea-

[a]*Department of Chemistry, University of Alberta, Edmonton, Alberta T6G 2G2 Canada. Fax: 780-492-8231; Tel: 780-492-1854; E-mail: alex.brown@ualberta.ca*

† Electronic Supplementary Information (ESI) available: Models of the studied chromophores (Figure S1), dihedral angles of the RFP-chromophore in a set of crystal structures representing the twist, tilt and 3 dihedrals in the extended acylimine conjugation (Table S1), coordinates of the optimized chromophore models (Table S2), data and differences between properties computed via B3LYP and CAM-B3LYP for the RFP- and GFP- derived models (Tables S3, S4, S7 and S8), gas-phase TD-DFT data (Table S5 and Figure S2), TPA cross sections calculated via the 2-level model and its components for the RFP-derived models (Table S6 and Figure S3), Λ-diagnostic for the first excitation of the RFP-derived models (Table S9), TD-DFT data for a subset of the chromophores at various acylimine dihedral angles (Tables S10 - S12), TPA cross sections calculated via the 2-level model and its components for Model 21 at conformers of varying acylimine dihedral angle (Table S13 and Figure S4), TD-DFT data for Model 21 at varying tilt and twist angles (Table S14), and plots for the variation of OPA oscillator strengths with varying tilt and twist angles (Figure S5). See DOI: 10.1039/b000000x/

surements for the same FP; for example, measurements made for the lower energy peak of an enhanced green-fluorescent protein (EGFP)[14] range from 1.5 GM[15] to 180 GM.[16] In any case, while large deviations may occur measurement-to-measurement, the experimental TPA spectra of the FPs consistently exhibit two regions of absorption: one at roughly double the wavelength of the OPA peak and another, stronger band shifted to a shorter wavelength.[13,17] The longer wavelength band is blue-shifted relative to double the wavelength of the corresponding OPA peak in the anionic chromophore spectra due to the enhancement of a vibronic transition.[18–21] The peak at a longer wavelength was determined theoretically as the excitation to the first (electronic) excited-state, S_0 to S_1, while the second, higher energy peak corresponds to a transition to a higher excited-state, S_0 to S_n. The main focus of this study, however, is on the S_0 to S_1 absorptions, as they occur in the near IR-region, and thus are more pertinent to imaging. Proteins of orange to far-red fluorescence have efficient TPA in the range between 1,000 nm and 1,200 nm (beyond the tuning range for Ti:sapphire lasers) where there is higher tissue transparency, weak scattering and very little autofluorescence.[13] Measurements of TPA cross-sections of a series of RFPs showed how the protein environment strongly affects the TPA of the chromophore.[13] Although they have the same chromophore structure (see the RFP chromophore model in Figure 1), the first bright state of mTangerine[22] has a measured TPA cross-section of 15 GM while that of a monomer of tdTomato[22] is 139 GM.[13]

The computation of TPA cross-sections is likewise challenging. Time-dependent density functional theory (TD-DFT) is used extensively to compute TPA cross-sections for large molecules due to its reasonable computational expense and relatively good accuracy.[17,19,23–29] Until recently, higher level ab initio methods were restricted only to the study of the TPA of small molecules. An investigation into the yellow fluorescent protein (YFP) showed that the CAM-B3LYP functional yields similar qualitative TPA results to the resolution-of-identity (RI) CC2 method.[26] Another study that compared TDDFT and full CC2 results showed that the B3LYP functional with the modest 6-31+G(d,p) basis can be used for a semi-quantitative comparison of TPA for the lowest energy excitation of FP chromophores.[30,31] Beerepoot et al. duly benchmarked CAM-B3LYP and RI-CC2 results against equation-of-motion CCSD (EOM-CCSD)[32–34] for a set of neutral FP chromophores.[35] Their results show that CC2 results are slightly overestimated as compared to EOM-CCSD ones within a factor of 1.4 while CAM-B3LYP results are significantly underestimated by a factor of 1.5 to 3.[35]

In recent years, great strides have been made in protein engineering following the development of methods to incorporate non-canonical amino acids (ncAAs) into proteins.[36–40] Barring ongoing research, only OPA has been experimentally explored for FPs containing ncAAs:[41–49] for example, the Gold FP (GdFP) - based off of the enhanced cyan FP (ECFP) with the replacement of Trp56 and Trp57 with a ncAA - saw a significant red-shifted emission compared to the ECFP as a result of the ncAA substitutions.[43] While ncAA incorporation can have a direct effect on chromophore structure, it can also have an indirect effect on the nature of excitation and/or emission when placed outside the central chromophore.[50] Important to realize, however, is that ncAA incorporation remains a difficult task. Consequently, each ncAA incorporated must ultimately generate a protein with sufficiently differing or enhanced functionality.

In a previous paper,[51] 22 chromophore models (constructed from the replacement of the Tyr66 residue of the tri-peptide precursor of a GFP template chromophore with a ncAA) were screened for excited-states properties; mainly TPA. Molecular dynamics simulations were further run to test the stability of a proposed FP containing the chromophore with maximal TPA cross-section (a nitro-substituted chromophore; similar to Model 22 in Figure 1). Recently, interest into mutating red-fluorescent proteins (RFPs) with ncAAs has been piqued.[52] In the present work, we computed OPA and TPA properties for the same set of 22 chromophores considered previously,[51] each of them now having an acylimine moiety resembling the extra maturation step in the RFPs. As the RFP chromophores occur in various conformations in reported crystal structures, we explore the effect of rotating the carbonyl of the acylimine moiety on the OPA and TPA of the chromophores with relatively large TPA cross-sections. We further investigate the effect of altering the tilt and twist angles between the rings of the chromophore with the largest intrinsic TPA cross-section. Inter-functional comparison between the TPA cross-sections computed by B3LYP and CAM-B3LYP is presented. We also compare our findings to the previous data[51] from GFP-derived chromophores.

2 Computational Methods

The chromophore structures were adopted from our previous work[51] with two modifications: (1) an extra extension is added to account for the acylimine moiety characteristic of RFP; (2) the broken connections between the chromophore and the rest of the protein are capped by methyl groups rather than hydrogen atoms. A subset of the chromophores considered is shown in Figure 1 while the full list is given in Figure S1 in the ESI†. Within the protein shell, the carbonyl of the acylimine is not coplanar with the rings of the chromophore, as observed in the crystal structures we analyzed (see the discussion in Section 3.2 and Table S1 in the ESI†). Hence, methyl capping is necessary when RFP-based chromophores are optimized to avoid obtaining a planar structure which would be far from the conformation (potentially) dic-

tated by the protein shell.[30] For the models with large TPA cross-sections, the effect of acylimine rotation on the TPA is further investigated.

We followed our previous protocol for optimization and computation of excited-states properties:[30,51] Dipole moments used in the two-level model (2LM) analysis were computed with DALTON[53] (2016 version) while all other computations were done with GAMESS-US (May-2013 version).[54] Optimization was done in the gas phase using the PBE0 functional.[55,56] The optimized coordinates for all structures are given in Table S2 of the ESI†.

Excited-state properties were computed with TD-DFT[57] within the response theory framework; OPA oscillator strengths (OS) and energies were computed via linear response,[58] while the two-photon transition matrix elements and the difference between permanent dipole moments of the excited and ground states were evaluated from the single and double residues of the quadratic response function,[59–62] respectively.

Assuming linearly polarized light, the transition moment for TPA is

$$\delta^{\mathrm{TPA}} = \frac{1}{15}\sum_{\alpha\beta}[S_{\alpha\alpha}S^{*}_{\beta\beta} + 2S_{\alpha\beta}S^{*}_{\alpha\beta}], \quad (1)$$

where the elements of the two-photon transition matrix are given by:

$$S_{\alpha\beta} = \sum_{n}\left[\frac{\langle 0|\mu_\alpha|n\rangle\langle n|\mu_\beta|f\rangle}{\omega_n - \omega} + \frac{\langle 0|\mu_\beta|n\rangle\langle n|\mu_\alpha|f\rangle}{\omega_n - \omega}\right]. \quad (2)$$

In Eq. 2, μ_α and μ_β refer to the dipole moment operator in a given Cartesian direction (α,β=x, y and z), ω_n is the energy gap from the ground state, $|0\rangle$, to a given state $|n\rangle$, ω is the photon energy ($=\frac{\omega_f}{2}$) and $|f\rangle$ is the final excited state.

The TPA cross section, σ^{TPA} , is commonly reported in units of 10^{-50} cm^4 s molecule^{-1} photon^{-1} that is referred to as one GM (in honour of the work[63] of "Maria Göppert-Mayer"). From the TPA transition moment and excitation energies (ω_f) produced by GAMESS, the TPA cross-section is calculated in macroscopic units (GM) and properly scaled to match single-beam experiments by:

$$\sigma^{\mathrm{TPA}} = \frac{4\pi^2 a_0^5 \alpha}{c}\frac{\omega^2}{\Gamma}\delta^{TPA}, \quad (3)$$

where α is the fine structure constant, a_0 is the Bohr radius, c is the speed of light, ω is the photon energy ($=\frac{\omega_f}{2}$) and Γ is the broadening factor derived from a Lorenzian function and chosen to be 0.1 eV for comparison with experiment, as previously employed.[23,30,64]

TPA computations were done using the conductor-like polarizable continuum model (referred to herein as PCM)[65–68] with parameters for water. Gas-phase TPA computations were used for comparison. The B3LYP functional[69] was mostly used for excited-states properties, while CAM-B3LYP[70] was used for comparison, as noted. The basis set 6-31+G(d,p)[71–75] in Cartesian form, i.e., 6 d-functions, was used in all computations.

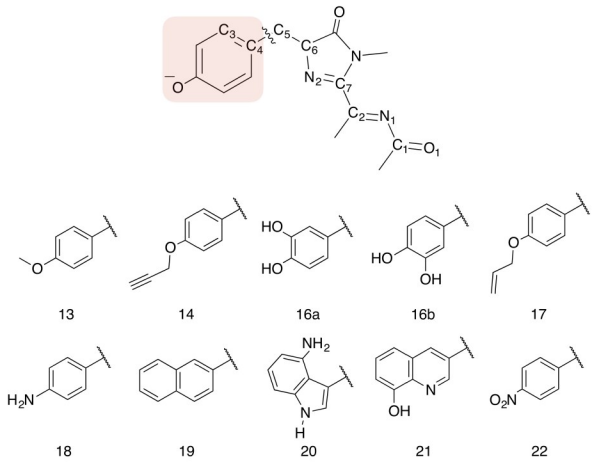

Fig. 1 A RFP chromophore model showing various angles that were varied in the TPA conformational study. The dihedral angle of the acylimine moiety ($\theta_{\mathrm{acylimine}}$) is made by atoms O_1, C_1, N_1 and C_2. The twist angle is the dihedral between atoms C_3, C_4, C_5 and C_6 while the tilt angle is the dihedral between atoms C_4, C_5, C_6 and N_2. Model chromophores are generated by replacing the highlighted part with moieties derived from nCAAs. A subset of these moieties is given below the parent structure while the full list is given in Figure S1 in the ESI†.

3 Results and Discussion

There are some important limitations associated with studying the TPA of isolated FP chromophores. Firstly, the protein environment has a large influence on its TPA through the following factors: (1) a steric factor affecting the conformation of the chromophore, (2) protein-chromophore interactions via residues that are in the vicinity of the chromophore, and (3) the electric field surrounding the chromophore.[4,13] Two previous computational studies of TPA accounted for the environmental effects via polarizable embedding (PE) mixed quantum mechanics and molecular mechanics (QM/MM) approaches.[21,28] Both studies confirmed the enhancement of TPA of the chromophore when embedded in the protein shell. Although all environmental factors affecting the TPA of the chromophore were theoretically considered, the first study on GFP did not quantitatively reproduce the experimental TPA spectrum.[28] Further, List et al. computed (at the CAM-B3LYP/6-31+G(d) level of theory) the TPA cross-section for the isolated RFP

chromophore of DsRed[4] at its vacuum-optimized geometry (17 GM), its protein-influenced geometry (47 GM), and for the whole protein via PE (106 GM).[21] The PE result was in good agreement with the experimental value (96 GM).[76] Including effective external field effects (due to the external electromagnetic field), however, nullified the enhancement due to the protein environment and caused the computed cross-section (30 GM) to fall even below that of the isolated chromophore (at its native protein conformation).[77] From these attempts, it seems that the computational toolbox needs more validation before it can reliably predict the quantitative effect of the protein environment on the TPA cross-section of the chromophore. In this work, we span some of the conformational space for the chromophore, based on our previous classical dynamics study[51] and data from crystal structures (Table S1 in the ESI†). Electrostatic effects from the protein shell or close-by residues are not considered. Secondly, we limit our study to vertical excitations and thus temperature and non-Condon effects are not considered. The present TD-DFT scan highlights promising chromophores with large intrinsic TPA cross-sections that might stimulate experimental interest.

The oxygen of the acylimine moiety is below the plane of the molecule in the optimized structures (coordinates given in Table S2 in the ESI†). In this conformation, the acylimine dihedral angle ($\theta_{\text{acylimine}}$ in Figure 1) is less than 180° which is similar to the angles found in the majority of the studied RFP-like crystal structures (Table S1 in the ESI†). We first discuss the OPA and TPA properties for the chromophores at their optimized conformations (Section 3.1). We then explore the change of TPA cross-section with the acylimine angle for some of the chromophores with relatively large cross-sections (Section 3.2). Finally, we compute the TPA cross-sections for a portion of the accessible conformational space of the chromophore with the largest TPA (Model 21) at fixed acylimine dihedral angles (Section 3.3).

3.1 TPA cross-sections

One-photon energies, OPA oscillator strengths, and the TPA cross-sections (corresponding to the transition to S_1, computed with B3LYP) for all chromophores are given in Table 1. Other data, including previous results of the GFP-derived chromophores[51] and comparison between the GFP and the RFP-derived ones, are given in Tables S3 and S4 in the ESI†. The comparison between the gas phase and PCM results in Table S5 and Figure S2 in the ESI demonstrate that the computation is not sensitive to the dielectric constant of the medium. As expected, the extra acylimine moiety results in a red-shift for the absorption of all chromophores (as compared to their GFP-derived counterparts).[51] The average red-shift is 0.446 eV, and Model 5 (a fluoro-derivative) has the maximum shift (0.522 eV). In terms of wavelengths, Model 20 (the Gold FP derivative) has the largest red-shift of 93 nm from 461 nm (2.689 eV)[51] to 554 nm (2.239 eV) corresponding to the GFP-derived and RFP-derived models, respectively.

In general, introducing the acylimine moiety is accompanied by an increase in TPA cross-section, as illustrated in Figure 2. Within the 2LM approximation, the sum-over-states (SOS) expression in Equation 2 becomes:[9,78]

$$\begin{aligned} S_{\alpha\beta} &= \frac{2}{\omega_1}[\mu_{\beta_{01}}(\mu_{\alpha_{11}}-\mu_{\alpha_{00}})+\mu_{\alpha_{01}}(\mu_{\beta_{11}}-\mu_{\beta_{00}})] \\ &= \frac{2}{\omega_1}[\mu_{\beta_{01}}(\Delta\mu_\alpha)+\mu_{\alpha_{01}}(\Delta\mu_\beta)], \end{aligned} \quad (4)$$

where $\mu_{\alpha_{mn}}$ is the α^{th} component of the dipole moment vector from state $|m\rangle$ to state $|n\rangle$; i.e., $\langle m|\mu_\alpha|n\rangle$, and ω_1 is the energy gap to the first excited state, $|1\rangle$. The difference between the permanent dipole moments of the first excited state and the ground state for the α^{th} component is denoted $\Delta\mu_\alpha$. As previously derived,[78,79] Equation 4 can be inserted in Equation 1 and manipulated using the vector nature of the dipole moment elements to give:

$$\delta^{\text{TPA}} = \frac{16}{15}\left(\frac{|\mu_{01}||\Delta\mu|}{\omega_1}\right)^2(2\cos^2\theta+1), \quad (5)$$

where θ is the angle between the μ_{01} and the $\Delta\mu$ vectors. Within the 2LM, equations 3 and 5 show that the increase in TPA cross-section can be due to larger μ_{01}, $\Delta\mu_{01}$ or having both vectors more aligned. The square of the transition dipole moment to the excited state is directly related to the corresponding OPA oscillator strength. There was slight variation in OPA oscillator strengths (within ±14%) upon the inclusion of the acylimine moiety except for Models 19, 20 and 21 where it increased by 0.24 (44%), 0.12 (33%) and 0.17 (55%), respectively. The average percent change in TPA cross-sections is 1227% while that of OPA oscillator strengths is 4%. In 13 models (approximately half of the studied set), the increase in TPA cross-section is actually accompanied by a decrease in OPA oscillator strength. In Models 11 and 15, the percent decrease in TPA cross-section was approximately 16 times the decrease in OPA oscillator strength. In Model 22, the TPA cross-section decreased by 35%, while the OPA oscillator strength increased by 8%. The percent increase of OPA oscillator strengths in Models 19 (44%), 20 (33%) and 21 (55%) is still significantly less than that of the TPA cross-sections (228%, 228% and 154%, respectively). It can thus be inferred that the change in TPA cross-sections is mainly driven by the change in permanent dipole differences ($\Delta\mu$) and not the change in transition dipole moments. The factors in Equation 5 are explicitly computed in the gas phase at the B3LYP and CAM-B3LYP/6-31+G(d,p) levels of theory and the complete set of results is reported in Table S6 and Figure S3 in the ESI†. A comparison between the TPA cross sections obtained via quadratic response and the truncated SOS approach

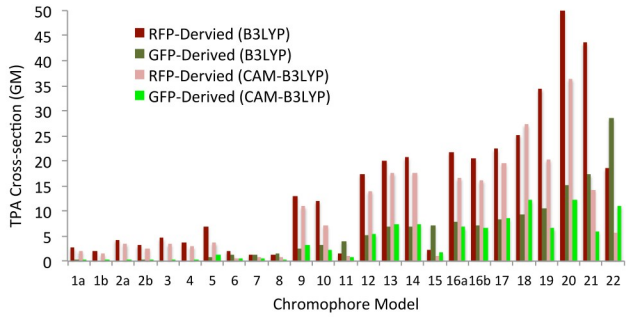

Fig. 2 TPA cross-sections of the GFP- and RFP-derived chromophores for the transition to S_1 as determined at the B3LYP/6-31G+(d,p) and the CAM-B3LYP/6-31G+(d,p) levels of theory with PCM (H_2O). For B3LYP, cross-sections of the RFP- and GFP-derived chromophores are given in Table 1 and taken from our previous work,[51] respectively. The data for cross-sections computed with CAM-B3LYP are given in Table S7 in the ESI†.

(within the 2LM) using the B3LYP functional is shown in Figure 3. The 2LM successfully captures the trend of relative TPA cross sections while there are deviations in terms of absolute values. Interestingly, the CAM-B3LYP results (see Figure S3 in the ESI) show a better agreement between the quadratic response and 2LM absolute values (with the exception of Model 21). The interplay between the three components affecting the 2LM cross sections is shown in Figure S3. While the transition dipole moment is nearly unchanged for most chromophores, the models with larger $\Delta\mu$ and with more aligned μ_{01} and $\Delta\mu$ vectors yield the largest cross sections. Models 16a through 22 have nearly aligned μ_{01} and $\Delta\mu$ vectors ($\cos^2\theta > 0.8$). Model 20 and, according to the B3LYP results, Model 21 get their special TPA enhancement due to the relatively large magnitude of $\Delta\mu$. Deviations from the 2LM, especially for Model 21, strongly suggest the involvement of channel interference[78] via higher excited states to the overall TPA cross-section of the relevant models; the detailed analysis of the photophysics within N-level (N > 2) models is beyond the focus of the present work.

The CAM-B3LYP functional has been shown to significantly underestimate the TPA strength of neutral chromophores as compared to the more accurate CC2 method.[26,35] A previous benchmark showed that the B3LYP functional seemed to (slightly) underestimate the TPA even more than CAM-B3LYP (a difference of less than 3 GM, according to the properly scaled values).[30,31] As there is a growing interest to benchmark the performance of CAM-B3LYP,[26] we computed the same properties for the same set of GFP- and RFP-derived chromophores using the CAM-B3LYP functional. Full data can be found in Table S7 in the ESI†. A comparison between the TPA results computed with CAM-B3LYP/6-31G+(d,p)

Model	Energy [eV]	OS	TPA [GM]
1a	2.977 (-0.478)	0.64 (0.00)	3 (2)
1b	2.987 (-0.481)	0.61 (-0.07)	2 (2)
2a	2.968 (-0.505)	0.67 (0.02)	4 (4)
2b	2.995 (-0.457)	0.63 (0.08)	3 (3)
3	2.968 (-0.495)	0.68 (-0.03)	5 (4)
4	2.923 (-0.464)	0.75 (-0.03)	4 (4)
5	2.945 (-0.522)	0.70 (0.00)	7 (6)
6	2.881 (-0.316)	0.83 (-0.08)	2 (0)
7	2.819 (-0.381)	0.88 (-0.05)	1 (0)
8	2.883 (-0.421)	0.75 (-0.05)	1 (0)
9	2.897 (-0.506)	0.82 (-0.03)	13 (11)
10	2.898 (-0.471)	0.81 (-0.04)	12 (8)
11	2.859 (-0.397)	0.78 (-0.03)	1 (-3)
12	2.772 (-0.438)	0.92 (-0.07)	17 (12)
13	2.785 (-0.504)	0.83 (-0.02)	20 (13)
14	2.801 (-0.509)	0.85 (-0.04)	21 (14)
15	2.840 (-0.382)	0.80 (-0.04)	2 (-5)
16a	2.733 (-0.485)	0.64 (0.06)	22 (14)
16b	2.783 (-0.477)	0.77 (0.06)	20 (13)
17	2.775 (-0.509)	0.86 (-0.04)	22 (14)
18	2.630 (-0.507)	0.91 (-0.02)	25 (16)
19	2.732 (-0.406)	0.80 (0.24)	34 (24)
20	2.239 (-0.450)	0.48 (0.12)	50 (35)
21	2.654 (-0.331)	0.46 (0.17)	44 (26)
22	2.710 (-0.255)	0.69 (0.05)	19 (-10)

Table 1 One-photon excitation energies [in eV], OPA oscillator strengths and TPA cross-sections [in GM] for the transition to S_1 as determined at the B3LYP/6-31G+(d,p) level of theory and PCM with parameters for H_2O. Between brackets is the difference between the property computed for the RFP-derived chromophore and that previously computed for the corresponding GFP-derived chromophore.[51]

in PCM (H_2O) for the GFP-derived and RFP-derived chromophores is shown in Figure 2 together with the analogous B3LYP computations; all TDDFT results are determined at the PBE0/6-31+G(d,p) optimized geometries (see Table S8 in the ESI†). Similar to the B3LYP results, the RFP-derived chromophores have larger TPA cross-sections than their GFP-derived counterparts (with some exceptions). The distribution of TPA cross-sections with CAM-B3LYP is of similar qualitative nature to that of B3LYP and both functionals agree that the RFP-derived form of Model 20 has the largest intrinsic TPA strength (at the optimized geometry). Contrary to B3LYP,[51] CAM-B3LYP does not predict that the nitro derivative (Model 22) has the largest TPA cross-section amongst the GFP-derived models. Opposing the trend previously observed on natural chromophores,[30] the TPA cross-sections computed by CAM-B3LYP are 1 to 3 times smaller than those computed by B3LYP (corresponding to a difference of 1 to 29 GM).

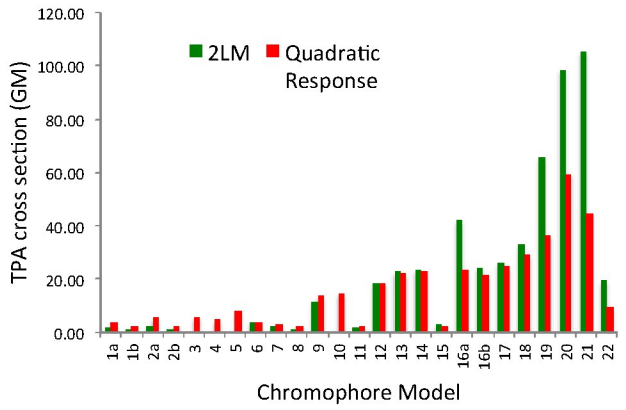

Fig. 3 TPA cross sections calculated via the components of the 2-level model (2LM) and via quadratic response at the B3LYP/6-31+G(d,p) level of theory in the gas phase. The contributing components to the 2LM expression are given in Table S6 in the ESI†.

The largest variation in TPA cross sections is in Models 19, 20 and 21. To investigate the extent of charge-transfer in the studied excitations, the overlap quantity Λ is reported[80] for the S_0 to S_1 transitions of the RFP-derived models (see Table S9 in the ESI†). The Λ parameter is a non-unique diagnostic value (ranging from 0 to 1) that measures the degree of overlap between virtual and occupied orbitals for a given excitation where small values (<0.4) indicate evidence for long-range excitations. All chromophore models have a Λ-diagnostic value of greater than 0.6 indicating the absence of significant charge-transfer in the transitions to the first excited state.

3.2 TPA change with acylimine rotation

As various crystal structures for RFPs are examined, we note that the acylimine carbonyl always assumes an out-of-plane conformation with respect to the rest of the chromophore (See Table S1 in the ESI†). In this set of chromophores (from crystal structures), $\theta_{\text{acylimine}}$ ranges from 129° to 359°. In addition, the carbon and nitrogen of the acylimine extension are usually off-plane, as can be shown by studying the dihedral angles θ_1 (made by C_1, N_1, C_2 and C_7) and θ_2 (made by N_1, C_2, C_7 and N_2), respectively (see Figure 1). As given in Table S1 in the ESI†, θ_1 ranges from 91° to 284° while θ_2 ranges from 165° to 256°. For simplicity, we limit our conformational study of the extended acylimine to the rotation of $\theta_{\text{acylimine}}$ while keeping θ_1 and θ_2 at the computationally optimized (near-planar) values. The RFP-derived chromophores with relatively large TPA cross-sections ($\geq$ 19 GM) as computed with B3LYP were considered in the acylimine rotation scan. The role of out-of-plane conformation of the acylimine moiety in increasing the TPA cross-section of DsRed[4] was previously discussed.[21,30] To the best of our knowledge, no study considered a full rotation of the acylimine moiety of the RFP chromophore, so we also included chromophore models of DsRed (See Figure 1) and mBlueberry1[81]. The mBlueberry1 chromophore (BLB) is similar to that of DsRed, but with no substitution on the benzene ring, i.e., no O^-. The scan considered a full rotation of the carbonyl moiety where the excited-state properties were computed at 10° intervals. Full TD-DFT results for the S_0 to S_1 excitations are given in Table S10 in the ESI†. As the acylimine is rotated, the rest of the structure is not re-optimized. As shown in Figure 4, the TPA cross-sections follow an oscillatory behaviour with the rotation of the carbonyl of the acylimine moiety. The results given in Table S11 and plotted in Figure 4 are for the TPA cross-sections associated with S_0 to S_1 transition with some exceptions: in Model 22 and BLB, the first two excited states of the near-planar structures ($\theta_{\text{acylimine}}$ = 0°, 10°, 340° and 350°) are nearly-degenerate with the first state being dark while the second is bright (See Table S12 in the ESI†). For the conformer with $\theta_{\text{acylimine}} = 330°$, the magnitude of the OPA oscillator strength is divided among the two states, with the second state having a slightly larger value. For all these near-planar cases for Model 22 and BLB, we included the TPA cross-section of the S_0 to S_2 transition in Figure 4. With the exception of Model 22 (NO_2-substituted), peak TPA cross-section is achieved when the acylimine is coplanar with the molecule. The difference between the maximum and minimum TPA cross-sections is more than 50% of the maximum value in nearly all chromophores. Interestingly, the RFP model follows neither trends. Having relatively weak TPA, it is difficult to discern the relationship between the acylimine angle and TPA at this level of theory. The type of capping (CH_3 vs H) and the variation in bond lengths and angles cause slight variation in cross-sections that is more pronounced if the molecule has already low intrinsic TPA. To demonstrate this inadequacy, we repeated the scan using a H-capped model for RFP after optimizing it at the same level of theory adopted for the methyl-capped model. The rotational scan produced a very similar trend to the methyl-capped counterpart, but with a lower cross-section (see Figure 4). As the chromophore is optimized at a certain acylimine angle and not re-optimized upon its rotation, this introduces some "noise" in the TPA computation. This "noise" could be ignored only if the chromophore model has a large intrinsic TPA, as can be seen in the other models. As a side note, methyl capping does not always increase the TPA cross-section, as demonstrated by another scan done on model 21 with H-capping (see comparison in Figure 4). In addition, using CAM-B3LYP for the RFP chromophore reproduces the same B3LYP trend.

The driving force for the trend in TPA cross sections ob-

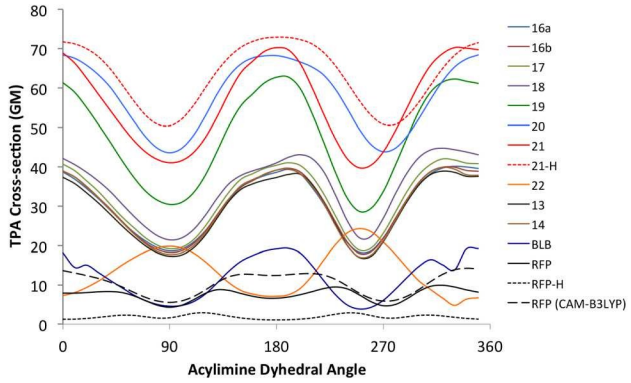

Fig. 4 Variation of TPA with rotation of the dihedral angle of the acylimine moiety ($\theta_{\text{acylimine}}$ in Figure 1). The TPA values are for the transition to S_1 (with some exceptions noted in the main text) as determined at the B3LYP/6-31G+(d,p) level of theory and PCM with parameters for H_2O. The dashed curve corresponds to a scan of the RFP model using CAM-B3LYP at the same level of theory. Only the two dotted curves were generated using H-capping while all other computations were done on CH_3-capped chromophores.

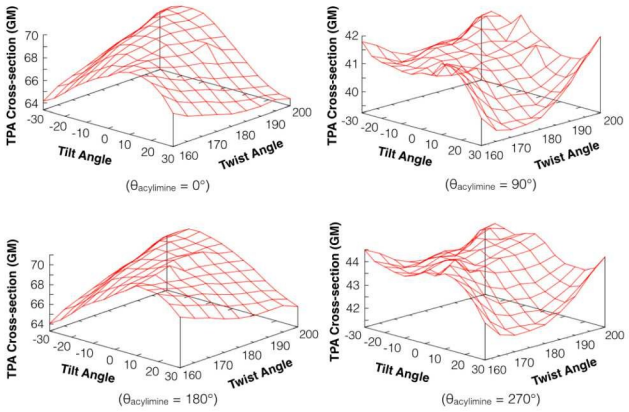

Fig. 5 Variation of TPA cross-sections with tilt and twist angles (see Figure 1) for Model 21 at fixed $\theta_{\text{acylimine}}$ of 0°, 90°, 180°and 270°. The TPA values are for the transition to S_1 as determined at the B3LYP/6-31G+(d,p) level of theory and PCM with parameters for H_2O.

served with the rotation of the acylimine dihedral of Model 21 was investigated. The components contributing to the TPA cross section within a 2LM were computed at the B3LYP and CAM-B3LYP/6-31+G(d,p) levels of theory in the gas phase for conformers of Model 21 varying $\theta_{\text{acylimine}}$ from 0° to 90° (with 10° intervals). Cross sections calculated via the truncated SOS approach within a 2LM follow the same oscillatory trend observed with the quadratic response results. Similar to what is discussed in Section 3.1, this trend is driven by the variation in $\Delta\mu$ and not in μ_{01}. Interestingly, B3LYP and CAM-B3LYP yield opposite trends for the alignment between the $\Delta\mu$ and μ_{01} vectors. Having the vectors nearly aligned under the studied spectrum of $\theta_{\text{acylimine}}$, the overall trend of TPA cross sections is the same whether computed by B3LYP or CAM-B3LYP. Relevant results are given in Table S13 and the significant trends are illustrated in Figure S4 in the ESI†.

3.3 TPA change with twist and tilt

Similar to what is observed in the acylimine moiety in the studied set of crystal structures, the rest of the chromophore body is usually distorted from planarity (See Table S1 in the ESI†). This distortion can be represented via the twist and tilt angles between the rings of the chromophore (see Figure 1). We computed the TPA of various tilt and twist angles for Model 21 which exhibits the largest intrinsic TPA (see Figure 4). Following our previous dynamics results,[51] the conformational flexibility of the chromophore is expected to range from -30°to +30°and from 160°to 200°for the twist and tilt angles, respectively. These angle ranges mirror those observed in the examined crystal structures for the proteins containing the RFP chromophore (See Table S1 in the ESI†). We varied the tilt and twist angles by 5°increments within these ranges at four fixed acylimine angles: 0°, 90°, 180°and 270°. Full data is available in Table S14 in the ESI. The change in TPA cross-section due to the variation of tilt and twist angles is less than 10% of the maximum TPA at a given acylimine dihedral (Figure 5). An interesting observation is that the OPA oscillator strength is maximum when the two rings are coplanar (regardless the value of $\theta_{\text{acylimine}}$) and this maximum value is maintained as the tilt angle is varied from 0°to 30°or to -30°as long as it is accompanied with a variation in the twist angle from 180°to 160°or to 200°, respectively (see Figure S5 in the ESI†). Nevertheless, energies and OPA oscillator strengths still experience relatively little total variation (within 0.1 eV and 0.17, respectively). These results, together with the results from Section 3.2, strongly suggest that the acylimine orientation is the strongest driver of change in the intrinsic TPA cross-sections for RFP-like chromophores.

4 Conclusion

In this work, we investigated the OPA and TPA properties for 22 RFP-like chromophores made from non-canonical amino acids. Interestingly, the extra acylimine moiety significantly alters the TPA cross-section of the chromophores along with the expected redshift in OPA energies. In terms of magni-

tude, the RFP-derived chromophores are determined to have larger TPA cross-sections than their GFP-derived counterparts that were previously computed.[51] Computing the TPA cross-sections with the B3LYP and CAM-B3LYP functionals yields similar trends but with some subtle quantitative differences. Results for both functionals at the optimized geometries agree that the RFP-derived Model 20 has the largest intrinsic TPA cross-section. The trend of TPA cross-sections as computed with PCM is mirrored by the gas-phase computation at the same level of theory. In addition, the simplified 2LM also reproduces the same trend computed via quadratic response. The 2LM analysis shows that the amplification of TPA cross-section in Model 20 is due to its relatively large $\Delta\mu$. Further, we studied the variation of TPA with the dihedral angle of the acylimine moiety ($\theta_{\text{acylimine}}$) for the models with relatively large TPA cross-sections and the natural RFP-like chromophores. We noticed a large variation of TPA with the rotation of the acylimine dihedral assuming an oscillatory trend that peaks at the planar conformation for all models except the nitro-substituted one (Model 22). The trend with $\theta_{\text{acylimine}}$ in the RFP chromophore is difficult to follow due to its low intrinsic TPA cross-section. Though larger than all other models, the TPA cross-sections determined for Models 21 and 20 are significantly lower at their optimized geometries (44 GM and 50 GM, respectively) than their planar conformations (70 GM and 68 GM, respectively). Studying the TPA trend for Model 21 with varying $\theta_{\text{acylimine}}$ using the 2LM reveals that the trend of cross-sections is, again, driven by the variation in $\Delta\mu$. We further computed the excited state properties for Model 21 with various tilt and twist angles spanning the most accessible conformational space. What is clear is that the acylimine angle has a much stronger effect on the TPA of the chromophore than its tilt and twist angles. Model 20 refers to a GdFP chromophore (but with the additional acylimine moiety) while Model 21 has a quinoline-like structure that has not yet been experimentally incorporated in a FP. Either model appears to be very promising in terms of intrinsic TPA cross-section that is more than 7 times that of the native RFP chromophore. In this work, we provide a rational basis to the experimental synthesis of FPs that are expected to have improved TPA cross-sections.

5 Acknowledgements

This work was supported by the Natural Sciences and Engineering Council of Canada (NSERC Discovery Grant to AB). This research was enabled through resources provided by Westgrid (www.westgrid.ca) and Compute/Calcul Canada (www.computecanada.ca).

References

1 O. Shimomura, F. H. Johnson and Y. Saiga, *J. Cell. Comp. Physiol.*, 1962, **59**, 223–229.
2 M. Ormo, A. B. Cubitt, K. Kallio, L. A. Gross, R. Y. Tsien and S. Remington, *Science*, 1996, **273**, 1392–1395.
3 F. Yang, L. G. Moss and G. Phillips, *Nat. Biotechnol.*, 1996, **14**, 1246–1251.
4 L. A. Gross, G. S. Baird, R. C. Hoffman, K. K. Baldridge and R. Y. Tsien, *Proc. Natl. Acad. Sci. U.S.A.*, 2000, **97**, 11990–11995.
5 R. M. Wachter, M. A. Elsliger, K. Kallio, G. T. Hanson and S. J. Remington, *Structure*, 1998, **6**, 1267–1277.
6 R. Weissleder, *Nat. Biotechnol.*, 2001, **19**, 316–317.
7 N. C. Shaner, P. A. Steinbach and R. Y. Tsien, *Nat. Methods*, 2005, **2**, 905–909.
8 R. Nifosì and V. Tozzini, *Fluorescent Proteins I*, Springer Berlin Heidelberg, 2012, vol. 11, pp. 3–40.
9 M. A. Salem, M. Gedik and A. Brown, in *Handbook of Computational Chemistry*, ed. J. Leszczynski, Springer Netherlands, Dordrecht, 2016, pp. 1–19.
10 C. Xu, W. Zipfel, J. B. Shear, R. M. Williams and W. W. Webb, *Proc. Natl. Acad. Sci. U.S.A.*, 1996, **93**, 10763–10768.
11 W. R. Zipfel, R. M. Williams and W. W. Webb, *Nat. Biotechnol.*, 2003, **21**, 1369–1377.
12 D. Oulianov, I. Tomov, A. Dvornikov and P. Rentzepis, *Opt. Comm.*, 2001, **191**, 235 – 243.
13 M. Drobizhev, N. S. Makarov, S. E. Tillo, T. E. Hughes and A. Rebane, *Nat. Methods*, 2011, **8**, 393–399.
14 G. Zhang, V. Gurtu and S. R. Kain, *Biochem. Biophys. Res. Commun.*, 1996, **227**, 707–711.
15 H. Hosoi, S. Yamaguchi, H. Mizuno, A. Miyawaki and T. Tahara, *J. Phys. Chem. B*, 2008, **112**, 2761–2763.
16 H. Kawano, T. Kogure, Y. Abe, H. Mizuno and A. Miyawaki, *Nat. Methods*, 2008, **5**, 373–374.
17 R. Nifosì and Y. Luo, *J. Phys. Chem. B*, 2007, **111**, 505–507.
18 Y. Ai, G. Tian and Y. Luo, *Mol. Phys.*, 2013, **111**, 1316–1321.
19 E. Kamarchik and A. I. Krylov, *J. Phys. Chem. Lett.*, 2011, **2**, 488–492.
20 M. Drobizhev, N. S. Makarov, S. E. Tillo, T. E. Hughes and A. Rebane, *J. Phys. Chem. B*, 2012, **116**, 1736–1744.
21 N. H. List, J. M. H. Olsen, H. J. A. Jensen, A. H. Steindal and J. Kongsted, *J. Phys. Chem. Lett.*, 2012, **3**, 3513–3521.
22 N. C. Shaner, R. E. Campbell, P. A. Steinbach, B. N. G. Giepmans, A. E. Palmer and R. Y. Tsien, *Nat. Biotechnol.*, 2004, **22**, 1567–1572.
23 R. Nifosì and Y. Luo, *J. Phys. Chem. B.*, 2007, **111**, 14043–14050.
24 L. Yuan, W. Lin, H. Chen, S. Zhu and L. He, *Angew. Chem., Int. Ed.*, 2013, **52**, 10018–10022.
25 F. Terenziani, C. Katan, E. Badaeva, S. Tretiak and M. Blanchard-Desce, *Adv. Mater.*, 2008, **20**, 4641–4678.
26 M. T. P. Beerepoot, D. H. Friese and K. Ruud, *Phys. Chem. Chem. Phys.*, 2014, **16**, 5958–5964.
27 M. G. Vivas, D. L. Silva, L. Misoguti, R. Zaleśny, W. Bartkowiak and C. R. Mendonca, *J. Phys. Chem. A*, 2010, **114**, 3466–3470.
28 A. H. Steindal, J. M. H. Olsen, K. Ruud, L. Frediani and J. Kongsted, *Phys. Chem. Chem. Phys.*, 2012, **14**, 5440–5451.
29 I. H. Nayyar and S. Tretiak, *J. Phys. Chem. C*, 2013, **117**, 18170–18189.
30 M. A. Salem and A. Brown, *J. Chem. Theory Comput.*, 2014, **10**, 3260–3269.
31 Note: In this benchmark, the reported TPA cross-sections were too large by a factor of 4 when given in macroscopic units (GM) due to the use of excitation energy (ω_f) in Equation 3 rather than photon energy ($\frac{\omega_f}{2}$).
32 J. F. Stanton and R. J. Bartlett, *J. Chem. Phys.*, 1993, **98**, 7029–7039.
33 R. J. Bartlett, *Mol Phys*, 2010, **108**, 2905–2920.

34 K. D. Nanda and A. I. Krylov, *J. Chem. Phys.*, 2015, **142**, 064118.
35 M. T. P. Beerepoot, D. H. Friese, N. H. List, J. Kongsted and K. Ruud, *Phys. Chem. Chem. Phys.*, 2015, **17**, 19306–19314.
36 N. Budisa, *Angew. Chem., Int. Ed.*, 2004, **43**, 6426–6463.
37 C. C. Liu and P. G. Schultz, *Ann. Rev. Biochem.*, 2010, **79**, 413–444.
38 J. A. Johnson, Y. Y. Lu, J. A. V. Deventer and D. A. Tirrell, *Curr. Op. Chem. Biol.*, 2010, **14**, 774 – 780.
39 M. G. Hoesl and N. Budisa, *Curr. Op. Biotechnol.*, 2012, **23**, 751 – 757.
40 R. B. Quast, D. Mrusek, C. Hoffmeister, A. Sonnabend and S. Kubick, *FEBS Lett.*, 2015, **589**, 1703 – 1712.
41 M. Taki, T. Hohsaka, H. Murakami, K. Taira and M. Sisido, *FEBS Lett.*, 2001, **507**, 35–38.
42 L. Wang, J. Xie, A. A. Deniz and P. G. Schultz, *J. Org. Chem.*, 2003, **68**, 174–176.
43 J. H. Bae, M. Rubini, G. Jung, G. Wiegand, M. H. Seifert, M. Azim, J.-S. Kim, A. Zumbusch, T. A. Holak, L. Moroder, R. Huber and N. Budisa, *J. Mol. Biol.*, 2003, **328**, 1071–1081.
44 P. P. Pal, J. H. Bae, M. K. Azim, P. Hess, R. Friedrich, R. Huber, L. Moroder and N. Budisa, *Biochem.*, 2005, **44**, 3663–3672.
45 D. Kajihara, T. Hohsaka and M. Sisido, *Protein Eng. Des. Sel.*, 2005, **18**, 273–278.
46 A. Goulding, S. Shrestha, K. Dria, E. Hunt and S. K. Deo, *Protein Eng. Des. Sel.*, 2008, **21**, 101–106.
47 F. Wang, W. Niu, J. Guo and P. G. Schultz, *Angew. Chem., Int. Ed.*, 2012, **51**, 10132–10135.
48 M. S. Padilla and D. D. Young, *Bioorg. Medicinal Chem. Lett.*, 2015, **25**, 470–473.
49 S. Chen, Z.-J. Chen, W. Ren and H.-W. Ai, *J. Am. Chem. Soc.*, 2012, **134**, 9589–9592.
50 S. M. Kuhn, M. Rubini, M. A. Müller and A. Skerra, *J. Am. Chem. Soc.*, 2011, **133**, 3708–3711.
51 M. A. Salem and A. Brown, *Phys. Chem. Chem. Phys.*, 2015, **17**, 25563–25571.
52 H.-W. Ai, private communication, Dec 2015.
53 *DALTON2016*, a molecular electronic structure program, 2016. Available online: http://www.daltonprogram.org.
54 M. W. Schmidt, K. K. Baldridge, J. A. Boatz, S. T. Elbert, M. S. Gordon, J. H. Jensen, S. Koseki, N. Matsunaga, K. A. Nguyen, S. J. Su, T. L. Windus, M. Dupuis and J. A. Montgomery, *J. Comput. Chem.*, 1993, **14**, 1347–1363.
55 J. P. Perdew, K. Burke and M. Ernzerhoff, *Phys. Rev. Lett.*, 1996, **77**, 3865–3868.
56 C. Adamo and V. Barone, *J. Chem. Phys.*, 1999, **110**, 6158–6169.
57 E. Runge and E. K. U. Gross, *Phys. Rev. Lett.*, 1984, **52**, 997–1000.
58 M. E. Casida, *Recent Advances in Density Functional Methods, Part I*, World Scientific, Singapore, 1995, ch. 5, pp. 155–192.
59 P. Sałek, O. Vahtras, J. Guo, Y. Luo, T. Helgaker and H. Ågren, *Chem. Phys. Lett.*, 2003, **374**, 446–452.
60 L. Frediani, Z. Rinkevicius and H. Ågren, *J. Chem. Phys.*, 2005, **122**, 244104.
61 S. Tretiak and V. Chernyak, *J. Chem. Phys.*, 2003, **119**, 8809–8823.
62 J. Olsen and P. Jørgensen, *J. Chem. Phys.*, 1985, **82**, 3235–3264.
63 M. Göppert-Mayer, *Ann. d. Phys.* 1931, **9**, 273–295.
64 P. Cronstrand, Y. Luo and H. Ågren, *Adv. Quantum Chem.*, 2005, **50**, 1.
65 V. Barone and M. Cossi, *J. Phys. Chem. A*, 1998, **102**, 1995–2001.
66 M. Cossi, N. Rega, G. Scalmani and V. Barone, *J. Comput. Chem.*, 2003, **24**, 669–681.
67 J. Tomasi, B. Mennucci and R. Cammi, *Chem. Rev.*, 2005, **105**, 2999–3094.
68 M. Cossi and V. Barone, *J. Chem. Phys.*, 2001, **115**, 4708–4717.
69 A. D. Becke, *J. Chem. Phys.*, 1993, **98**, 5648–5652.
70 T. Yanai, D. P. Tew and N. C. Handy, *Chem. Phys. Lett.*, 2004, **393**, 51 – 57.
71 R. Ditchfield, W. J. Hehre and J. A. Pople, *J. Chem. Phys.*, 1971, **54**, 724–728.
72 W. J. Hehre, R. Ditchfield and J. A. Pople, *J. Chem. Phys.*, 1972, **56**, 2257–2261.
73 M. M. Francl, W. J. Pietro, W. J. Hehre, J. S. Binkley, M. S. Gordon, D. J. DeFrees and J. A. Pople, *J. Chem. Phys.*, 1982, **77**, 3654–3665.
74 P. Hariharan and J. Pople, *Theor. Chim. Acta*, 1973, **28**, 213–222.
75 T. Clark, J. Chandrasekhar, G. W. Spitznagel and P. V. R. Schleyer, *J. Comput. Chem.*, 1983, **4**, 294–301.
76 M. Drobizhev, S. Tillo, N. S. Makarov, T. E. Hughes and A. Rebane, *J. Phys. Chem. B*, 2009, **113**, 12860–12864.
77 N. H. List, H. J. A. Jensen and J. Kongsted, *Phys. Chem. Chem. Phys.*, 2016, **18**, 10070–10080.
78 M. M. Alam, M. Chattopadhyaya, S. Chakrabarti and K. Ruud, *Acc. Chem. Res.*, 2014, **47**, 1604–1612.
79 M. M. Alam, M. Chattopadhyaya and S. Chakrabarti, *Phys. Chem. Chem. Phys.*, 2012, **14**, 1156–1165.
80 M. J. G. Peach, P. Benfield, T. Helgaker and D. J. Tozer, *J. Chem. Phys.*, 2008, **128**, 044118.
81 H.-W. Ai, N. C. Shaner, Z. Cheng, R. Y. Tsien and R. E. Campbell, *Biochemistry*, 2007, **46**, 5904–5910.